Sensors and Actuators A 161 (2010) 152–157

Contents lists available at ScienceDirect

Sensors and Actuators A: Physical

journal homepage: www.elsevier.com/locate/sna

Numerical modeling of electro-conjugate fluid flows

Hideki Yamamoto[a], Kento Mori[b], Kenjiro Takemura[b,*], Leslie Yeo[c], James Friend[c], Shinichi Yokota[d], Kazuya Edamura[e]

[a] Graduate School of Science and Technology, Keio University, Japan
[b] Department of Mechanical Engineering, Keio University, Japan
[c] Micro/Nanophysics Research Laboratory, Department of Mechanical & Aerospace Engineering, Monash University, Australia
[d] Precision and Intelligence Laboratory, Tokyo Institute of Technology, Japan
[e] New Technology Management Co. Ltd., Japan

ARTICLE INFO

Article history:
Received 27 November 2009
Received in revised form 2 April 2010
Accepted 13 April 2010
Available online 7 May 2010

Keywords:
Functional fluids
Electro-conjugate fluids
Electrohydrodynamics
Particle image velocimetry
Microfluidics

ABSTRACT

An electro-conjugate fluid (ECF) is a kind of low conductivity dielectric fluid, which produces a strong flow when subjected to high DC voltage. ECFs are potentially useful in a variety of applications, including microactuators, microgyroscopes, and CPU liquid cooling systems. However, the biggest hindrance to the commercial development of applications involving ECFs is the lack of theoretical understanding of the fluid flow mechanisms associated with ECFs. This study presents a numerical simulation based on a physical model for the flow of ECFs that arises due to the generation of electric (Maxwell) stress gradients. Validation of the results from the numerical simulation against experimental data obtained using particle image velocimetry (PIV) provides confidence that the model is capable of quantitatively reproducing the flow of these ECFs.

1. Introduction

An "electro-conjugate fluid" or "ECF" is the generic name for a class of low conductivity dielectric functional fluids that can be propelled when subjected to a non-uniform electric field [1], as depicted in Fig. 1. By mapping the fluid flow characteristics in terms of its viscosity and conductivity, as shown in Fig. 2, it is possible to distinguish between the various fluids *in* the ECF family that exhibit strong flow under the applied non-uniform electric field, and the rest of the dielectric fluids *outside* the ECF family that do not exhibit such flow. It can be seen that the ECFs lie within a well-defined triangular area in the viscosity–conductivity space.

An attractive advantage of ECFs is the ability to generate fluid flow without mechanically-moving parts. Moreover, previous investigations have also indicated that the ECF flow intensity increases with a decrease in the size of the electrode pair [2], thus eliminating the need for the large conventional pumps required in pneumatic/hydraulic systems. In addition, this ability to miniaturize the system facilitates a convenient means for driving these fluids in micro-electro-mechanical-system (MEMS) and microfluidic devices [3–5], particularly in microcooling technologies [6].

While there are a broad range of mechanisms that give rise to electrohydrodynamic (EHD) phenomena [7], such as ion drag [8], conduction pumping [9] and induction pumping [10], recent work [11] has, however, shown that the flow of an ECF under an applied electric field does not appear to arise from these classical electrohydrodynamic mechanisms. Instead, it was proposed that the applied non-uniform electric field across the fluid gave rise to gradients in the electric (Maxwell) stress within the liquid, confirmed by the good agreement between the experimental data carried out in a microchannel configuration with a simple analytical model that accounted for the effects of the Maxwell stress [11].

Here, we provide further evidence to confirm that the EHD flow of ECFs can be described by the Maxwell stress gradient mechanism by extending the lubrication analysis in [11] to capture the ECF flow arising from the hollow ring and pin electrode configuration shown in Fig. 1. Since the large aspect ratio of microchannels can no longer be exploited to simplify the equations governing the fluid flow, the lubrication assumption is relaxed. An analytical solution is however no longer possible, and hence we carry out numerical simulations using a finite element technique and compare our results to the flow field description obtained experimentally via particle image velocimetry (PIV).

Section 2 details the underlying theory for ECF flow arising due to gradients in the Maxwell stress, which is then subsequently used in the numerical computation in Section 4. Experiments to obtain the flow velocity distribution PIV are briefly discussed in Section 3,

* Corresponding author at: 3-14-1 Hiyoshi Kohoku-ku Yokohama 223-8522 Japan, Tel.: +81 45 566 1826; fax: +81 45 566 1826.
E-mail address: takemura@mech.keio.ac.jp (K. Takemura).

0924-4247/$ – see front matter © 2010 Elsevier B.V. All rights reserved.
doi:10.1016/j.sna.2010.04.033

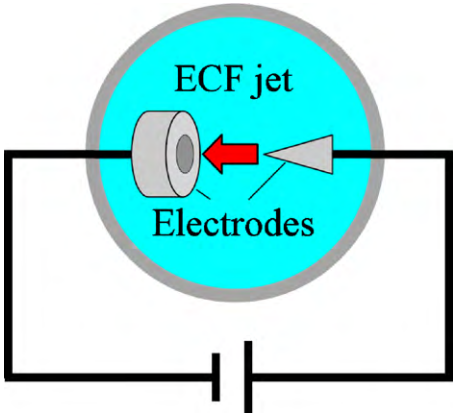

Fig. 1. Schematic depiction of the flow of an ECF when subjected to a non-uniform electric field arising across a pin and hollow ring electrode structure.

which are then the basis of a comparison with the results obtained via the numerical simulations.

2. Maxwell stress gradient model

An appropriate starting point is the electric body force density acting on a liquid, which can be described by the Korteweg–Helmholtz equation [12],

$$\mathbf{F}_e = q\mathbf{E} - \frac{1}{2}\mathbf{E}\cdot\mathbf{E}\nabla\varepsilon + \frac{1}{2}\nabla\left[\rho\left(\frac{\partial\varepsilon}{\partial\rho}\right)_T\right]\mathbf{E}\cdot\mathbf{E}, \quad (1)$$

where q is the net charge density of the bulk space charge in the fluid, ε the permittivity of the fluid, ρ its density, $\mathbf{E}$ the applied electric field vector, and T the temperature, respectively. Briefly, the first term accounts for the electric (Coulomb) force exerted on free charges in the liquid. The second term, on the other hand, accounts for a ponderomotive force [7] that is induced if a permittivity gradient exists, for example, across a liquid/vapor or liquid/liquid interface, or due to inhomogeneities that arise, for example, due to the existence of non-isothermal conditions. This force could also arise due to dipole polarization within the media, which consequently interact with the external field (as opposed to dipole–dipole interaction). Finally, the third term accounts for electrostrictive effects that usually accompanies compressible media.

For incompressible fluids in which the electrostrictive effect is insignificant, the flow therefore arises either due to the presence of space charges that experience an electric force when subjected to an applied electric field or if sufficient polarization arises due to

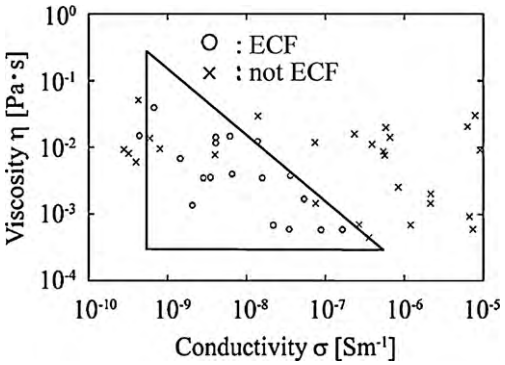

Fig. 2. Delineation of ECFs and non-ECFs according to their viscosities and conductivities. Fluids which exhibit strong flow under an applied non-uniform electric field are denoted by the circles and generally fall within the triangular area. These are termed as electro-conjugate fluids or ECFs. Those that do not exhibit such flow, as denoted by the crosses, generally tend to lie outside this triangular area.

the presence of induced charges (dipoles) when the electric field is applied. It should be noted that Eq. (1) generally applies to both electrolytes and dielectric liquids. The only difference that arises for electrolytes is that an electric double layer is formed in which space charge exists—this double layer screens the external field and produces an electro-osmotic slip velocity; no such phenomena exists in dielectric liquids, and hence an ECF flow which is generated must arise from a different mechanism [7].

The Coulombic and ponderomotive components of the body force in Eq. (1) can be described as a divergence of the Maxwell stress tensor,

$$\mathbf{T}_M = \varepsilon\mathbf{E}\mathbf{E} - \frac{\varepsilon}{2}(\mathbf{E}\cdot\mathbf{E})\mathbf{I}, \quad (2)$$

where $\mathbf{I}$ is the unit (identity) tensor, and, in turn, can be expressed as a scalar Maxwell pressure through the Gauss divergence theorem. Essentially, the Maxwell pressure causes a concurrent compression force and a transversal expansion force with respect to the electric field. Therefore, if the electric field is non-uniform, the total compression and expansion pressure exerted on the fluid do not cancel and hence this departure from equilibrium generates a net force that drives the fluid to flow [7,13].

The EHD flow can then be captured by including the Maxwell stress tensor in Eq. (2) in the total stress tensor acting on the fluid:

$$\mathbf{T} = -p\mathbf{I} + \mathbf{T}_v + \mathbf{T}_M, \quad (3)$$

where p is the fluid pressure and $\mathbf{T}_v$ is the viscous stress tensor, given by

$$\mathbf{T}_v = \mu[\nabla\mathbf{V} + (\nabla\mathbf{V})^T], \quad (4)$$

μ being the fluid viscosity and $\mathbf{V}$ the velocity field vector, where superscript T refers to a transpose. Given that the equation governing the equation of motion of an incompressible Newtonian fluid is

$$\rho\frac{D\mathbf{V}}{Dt} = \nabla\cdot\mathbf{T}, \quad (5)$$

where t denotes time and hence D/Dt is the material derivative, we then arrive at the final expression describing the EHD fluid flow,

$$\rho\frac{D\mathbf{V}}{Dt} = -\nabla p + \mu\nabla^2\mathbf{V} + \varepsilon\left[(\mathbf{E}\cdot\nabla)\mathbf{E} - \frac{1}{2}\nabla|\mathbf{E}|^2\right], \quad (6)$$

from which we observe the coupling between the electric field and the hydrodynamics, the origin of all EHD flow. Note the requirement for a field gradient and hence the existence of a non-uniform applied field. If the tangential field is weak, as in the case in [11] where the slender body or lubrication assumption can be invoked, then the off-diagonal terms arising from the mixed derivatives can be omitted and the electric field stresses can be written as a gradient of the Maxwell pressure [14]:

$$\rho\frac{D\mathbf{V}}{Dt} = -\nabla(p + p_M) + \mu\nabla^2\mathbf{V}, \quad (7)$$

where

$$p_M = \frac{E_n^2}{2}, \quad (8)$$

E_n being the normal component of the electric field.

3. Flow visualization

Fig. 3 shows the experimental setup used in this study and designed to mimic the hollow ring and pin electrode configuration illustrated in Fig. 1 that has a similar configuration and cross-sectional dimensions to past work [2,4,5]. The device consists of three brass electrodes and three acrylic resin boards. The electrodes with 1 mm × 1 mm cross-sections are inserted into alignment holes

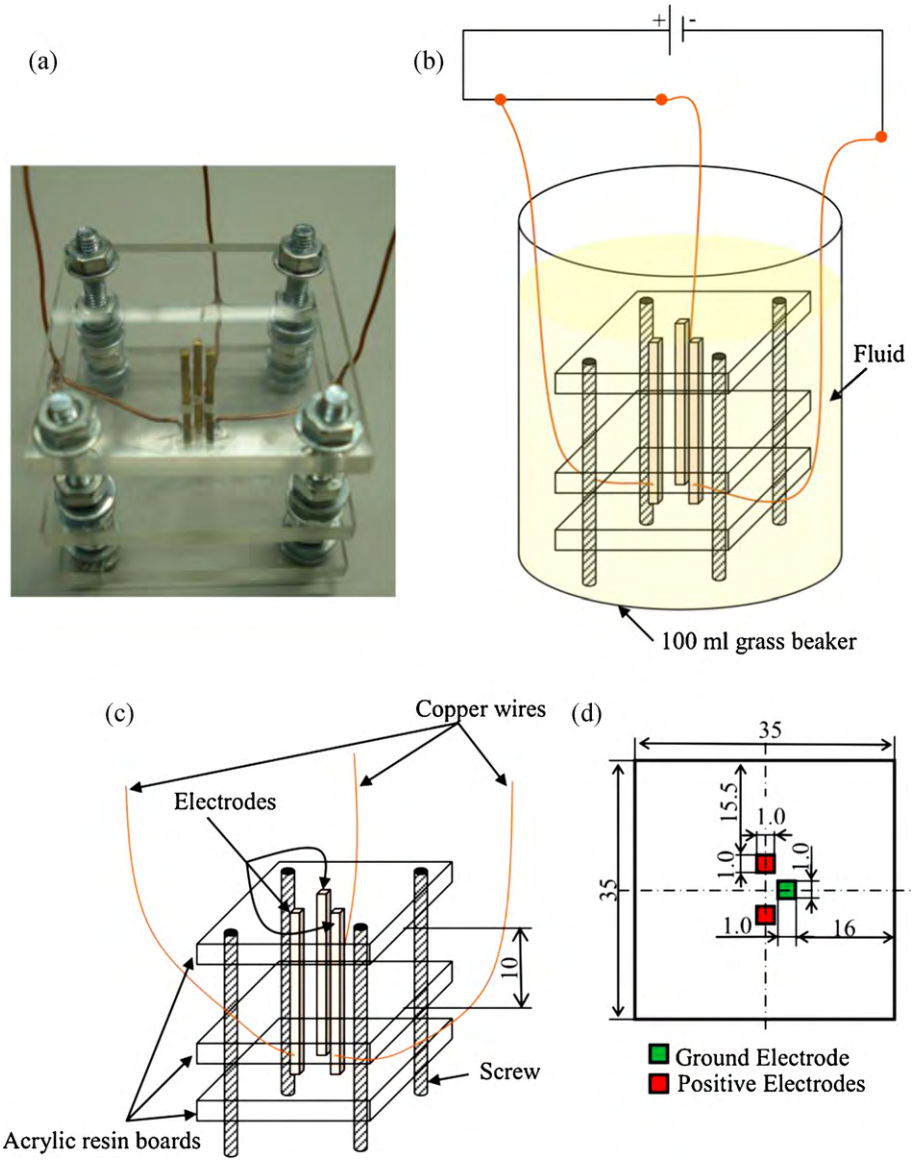

Fig. 3. Schematic representation of the experimental device; (a) actual view of electrodes, (b) showing how it is used, (c) the placement of the electrodes, and (d) the electrode as viewed from the top and their spacing.

on the acrylic resin boards. The gap between the top and middle acrylic resin boards is 10 mm forming a region where the fluid flows for visualization. The entire device is then immersed in the working fluid, housed in a 100 ml glass beaker. The working fluid comprises a particular type of ECF, FF-1_{EHA2} (New Technology Management Co. Ltd., Japan), whose physical properties are tabulated in Table 1.

The beaker is then placed on the vibration-free stage of an inverted fluorescence microscope (VH-Z00R, KEYENCE, Co. Ltd., Japan). Cross-linked polymethylmethacrylate or PMMA particles of 12 μm diameter (MBX-12, Sekisui Chemical Co. Ltd., Japan) are suspended in the working fluid with a concentration of 0.05 vol% to function as tracer particles for the flow visualization using the PIV technique. Relative density of PMMA is 1.2 (that of FF-1_{EHA2} is 1.7). The choice of the particle size is deliberate—it is sufficiently large such that the particle trajectories are not overwhelmed by Brownian motion but adequately small such that the presence of the particle does not significantly alter the macroscopic flow field. The flow field is observed with transmitted light using a 60 W metal halide lamp and captured using a high-speed camera (VW-100C, KEYENCE, Co. Ltd., Japan), capable of recording up to 24,000 frames/s; 1000 frames/s were employed in these experiments. The images were acquired along a plane at equidistant gaps (5 mm) from the top/middle acrylic boards, while the ECF flow was driven at 1.332 kV DC applied across the electrodes.

Fig. 4 shows the velocity distribution of the flow field, reconstructed from the still frame images acquired from the high-speed video recording using PIV software (VidPIV, Oxford Lasers Ltd., UK). We observe the existence of a strong flow from the corners of the ground electrode where a near-singular field exists towards the gap between the positive electrodes where a lower field intensity exists. This is consistent with previous observations where the flow direction is from the high field region to the low field region, consistent with the postulated Maxwell stress gradient flow mechanism [11].

Table 1
Physical properties of FF-1_{EHA2}.

Density	1688 kg/m^3
Viscosity	11 mPa S
Relative permittivity	5.2

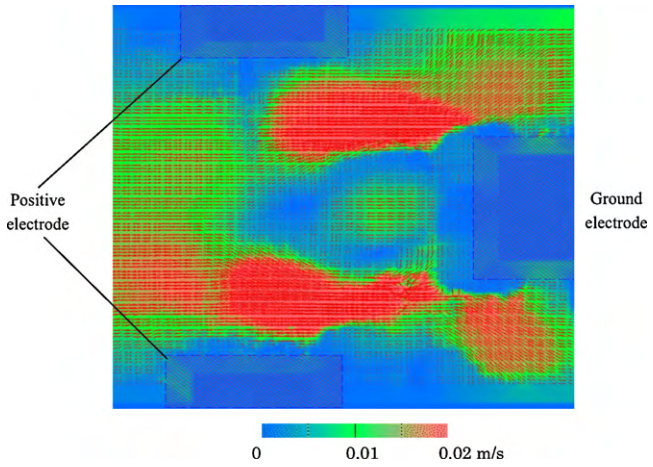

Fig. 4. Velocity distribution of the flow field reconstructed using PIV software from the trajectories of the seeded microparticles observed experimentally.

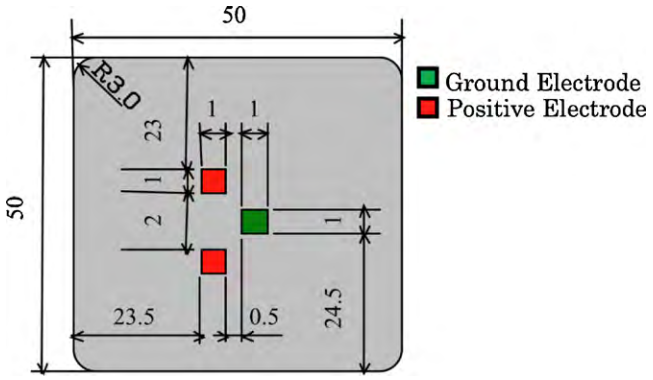

Fig. 5. Schematic illustration of the geometry of the two-dimensional numerical model (all units are in mm).

4. Numerical procedure

The geometry of the two-dimensional numerical model is intended to mimic the experimental device illustrated in Fig. 5. There are three square electrodes (1 mm × 1 mm), one is connected to the ground and the others are positive, located almost at the center of the analytical domain. The working fluid is the same as that used in the experiments, FF-1_{EHA2}, whose physical properties are given in Table 1, although any other fluid in the ECF family described by Fig. 2 could generally be employed. The dimension of the domain is set to be sufficiently large such that edge effects due to the presence of the boundary are negligible on the ECF flow generated in the electrode region.

Given that space charge can be neglected in low conductivity dielectric liquids, the electric potential φ can be obtained by solving

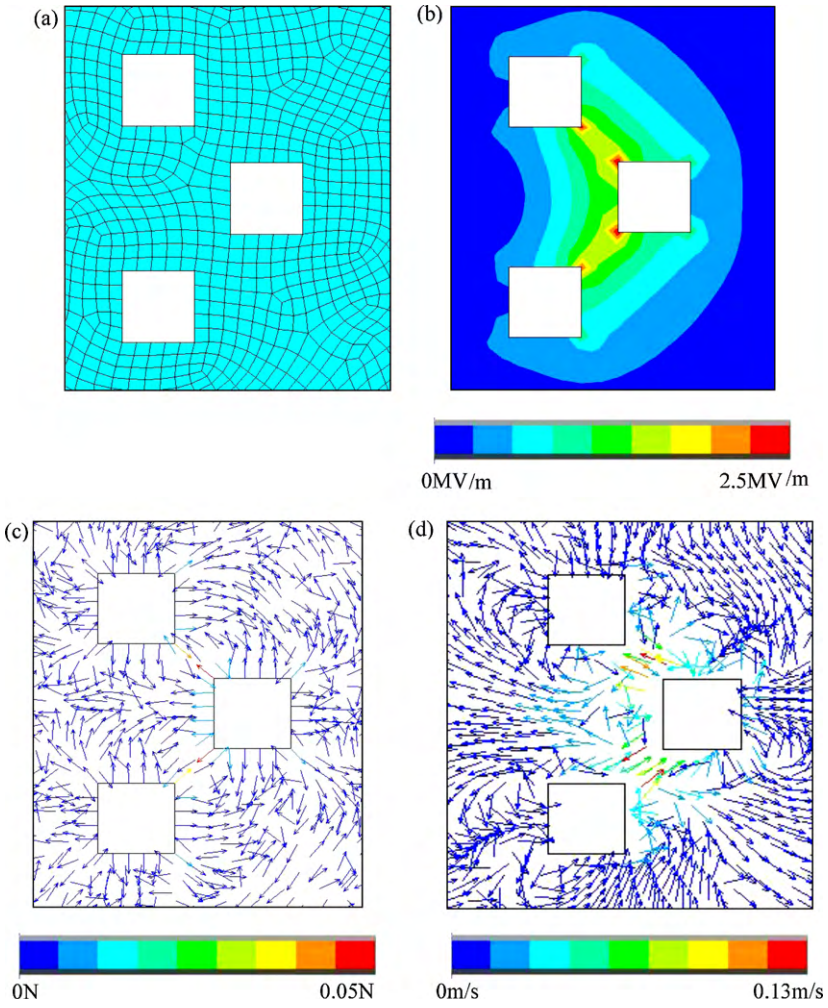

Fig. 6. Computed results from the finite element simulation for (a) finite elements, (b) the electric field, (c) the Maxwell force, and (d) the resulting fluid velocity.

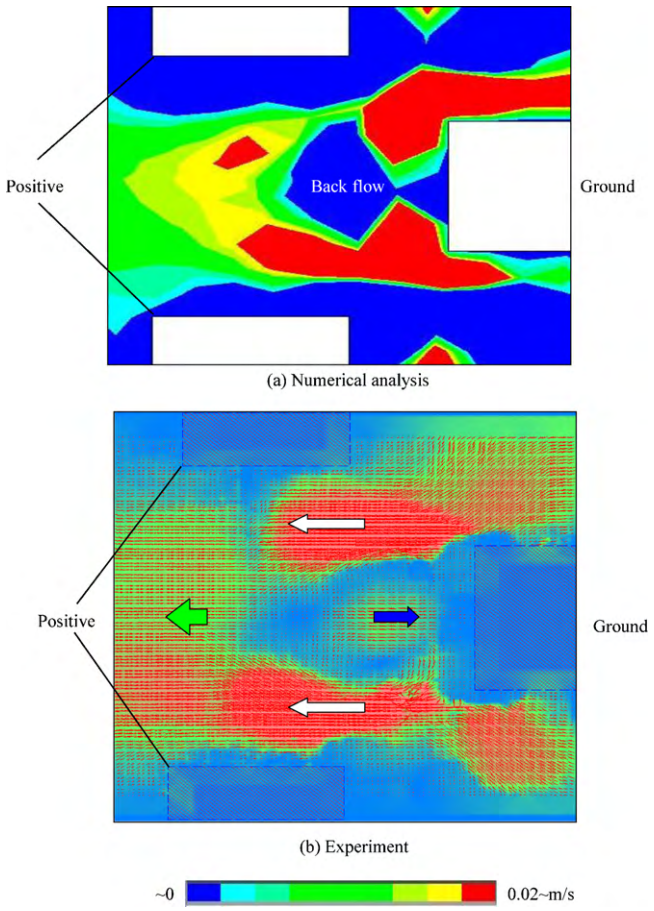

Fig. 7. Comparison between the ECF flow velocity distributions obtained (a) numerically and (b) experimentally.

the Laplace equation:

$$\nabla^2\varphi = 0, \tag{9}$$

from which the electric field $\mathbf{E} = -\nabla\varphi$ can be obtained. At the positive electrode, $\varphi = V$ (V = 1.332 kV corresponding to the experiments in Section 3) where V is the applied voltage, and at the ground electrodes, $\varphi = 0$. At the boundaries of the solution domain, we impose insulated boundary conditions $\partial\varphi/\partial n = 0$, n being the normal coordinate. In the absence of deformable boundaries and space charge, the electrostatic problem given by Eq. (9) can be solved separately and couples to the hydrodynamics via Eq. (6), which we solve numerically subject to no-slip conditions $\mathbf{V} = 0$ along all surfaces using the finite element software package ANSYS (ANSYS. Inc., USA). The domain was created using eight-node electrostatic solid elements for the electric field analysis and 2D fluid-thermal elements for the fluid analysis to generate a non-uniform mesh with up to 50,330 nodes, convergence of the numerical solution being ensured through mesh refinement. In ANSYS, the electromagnetic force was calculated using the result of electric field computation. Then the force is introduced to the hydrodynamic simulation as an external force. The hydrodynamic simulation is carried out over a period of 500 s over which the flow equilibrated towards steady state.

Fig. 6(a) shows the contours of the electric field, obtained by solving Eq. (9). The maximum value of the electric field strength is around 2.5 MV/m, which is smaller than the electric breakdown strength of FF-1_{EHA2}, at the sharp corners of the ground electrode, indicating the existence of a large field intensities in these regions. Fig. 6(b)shows the Maxwell force distribution, obtained by taking the divergence of the Maxwell stress tensor given by Eq. (2). The Maxwell force is observed to be oriented normally outwards from the electrodes, and reaches a maximum of 0.05 N at the sharp corners of the ground electrodes, as expected. Fig. 6(c) shows the corresponding velocity distribution of the ECF flow arising from the gradients in the Maxwell stress. We note the existence of a strong flow from the high field intensity region near the sharp electrode corners where a maximum flow velocity of 0.13 m/s is reached. Although this is slightly higher than the 0.02 m/s velocities measured experimentally(the maximum flow velocity is calculated in a tiny local area, which is difficult to be observed experimentally), the salient features of the flow are at least captured by the numerical model. This agreement can be more closely scrutinized in Fig. 7, from which we observe that the flow is driven from the high field regions near the corners of the ground electrode through the region in between the positive electrodes where the field intensity is low, again consistent with the postulated Maxwell stress gradient mechanism in earlier work carried out on ECF flow [11]. In addition, we observe in both the computed and observed velocity distributions the formation of a closed vortex in the region between the ground and positive electrodes due to the existence of a back- or counter-flow as the Maxwell stress gradient driven flow from both corners of the ground electrodes converges in the low field region in the gap between the positive electrodes. Note that the asymmetrical nature of the flow velocity distribution is based on the asymmetric meshes, which is automatically generated in ANSYS.

Fig. 8 shows the numerical and experimental flow velocity distributions with the different input voltage, 1.998 kV, which is

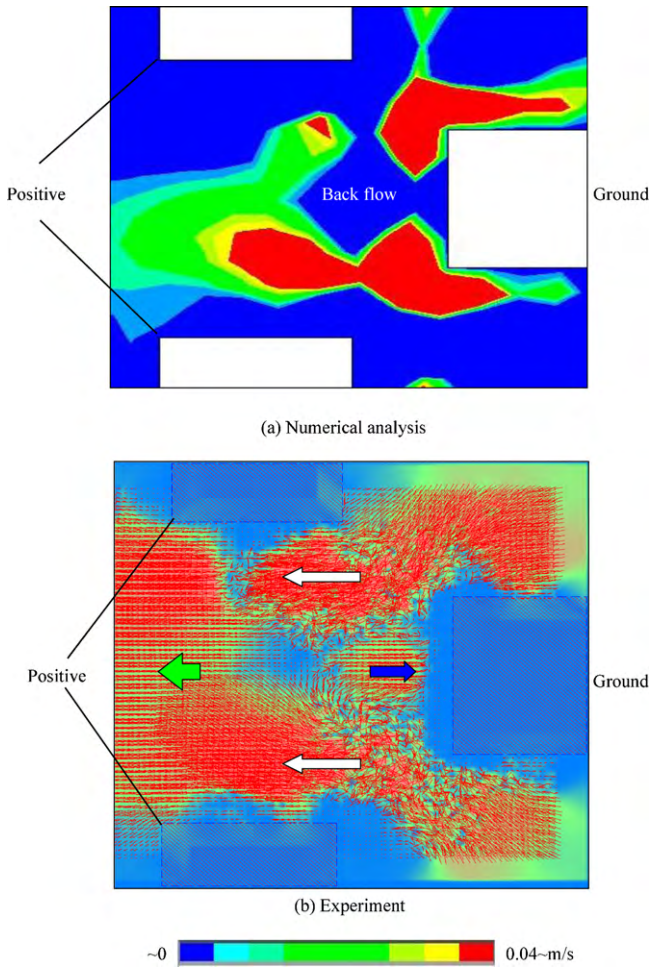

Fig. 8. Comparison between the ECF flow velocity distributions with 1.998 kV.

1.5 times higher than the above-mentioned experiment/numerical computation. Note that the other conditions are kept the same. These results again agree well each other. In addition, the flow velocity range becomes 2 times larger than that in Fig. 7. This roughly matches the square of voltage increase rate, because the Maxwell stress is proportional to E^2.

5. Conclusions

The work reported in this paper provides further empirical and numerical support for an earlier fundamental study on the dominant mechanism by which the flow of an electro-conjugate fluid arises under an applied non-uniform electric field [11]. Here, the one-dimensional lubrication analysis previously employed for a large aspect ratio microchannel ECF flow is relaxed and the full electrostatic and hydrodynamic equations are solved numerically using a two-dimensional finite element model to obtain the electric field, Maxwell force and corresponding velocity field for the flow of an ECF with a hollow ring and pin electrode configuration. The results of the numerical study are compared to experimental results of the flow field obtained using particle image velocimetry. A comparison between the numerical and experimental results shows that the salient features of the observed flow can be captured by the numerical model, with reasonable qualitative agreement. In particular, the flow is seen to be driven from the high field intensity region near the sharp ground electrode corners to the low field intensity region between the positive electrodes. Due to the convergence of the flow in this region, a back-flow emanates to give rise to a recirculating vortex in the region between the ground and positive electrodes. These flow characteristics are consistent with that in [11] and hence provide further support for the Maxwell stress gradient principle which was postulated as the fundamental underlying driving mechanism for ECF flow.

Acknowledgements

The work reported in this article was supported in part by the Japan Science and Technology Agency, a Grant-in-Aid for Encouragement of Young Scientists (A) #21686017 awarded by the Ministry of Education, Culture, Sports, Science and Technology of Japan, and the Japan Securities Scholarship Foundation.

References

[1] S. Yokota, Y. Otsubo, K. Edamura, Electro-sensitive Movable Fluids, Method of Using the Same and Motors for the Electro-sensitive Movable Fluids, USP 6,030,544, 2000.
[2] A. Ryutaro, K. Takemura, K. Edamura, S. Yokota, Concept of a micro-finger using electro-conjugate fluid and fabrication of a large model prototype, Sensors & Actuators A 136 (2) (2007) 629–637.
[3] K. Takemura, H. Kozuki, K. Edamura, S. Yokota, A micromotor using electro-conjugate fluid—improvement of motor performance by using saw-toothed electrode series, Sensors & Actuators A 140 (2007) 131–137.
[4] K. Takemura, F. Yajima, S. Yokota, K. Edamura, Integration of micro-artificial muscle cells using electro-conjugate fluid, Sensors & Actuators A 144 (2) (2008) 348–352.
[5] K. Takemura, S. Yokota, K. Imamura, K. Edamura, H. Kumagai, The practical design of a liquid rate gyroscope using electro-conjugate fluid, Journal of Systems and Control Engineering, Proceedings of the Institution of Mechanical Engineers Part I 233 (6) (2009) 727–736.
[6] W.-S. Seo, K. Yoshida, S. Yokota, K. Edamura, A high performance planar pump using electro-conjugate fluid with improved electrode patterns, Sensors & Actuators A 134 (2) (2007) 606–614.
[7] H.-C. Chang, L.Y. Yeo, Electrokinetically Driven Microfluidics and Nanofluidics, Cambridge University Press, New York, 2010.
[8] O.M. Stuetzer, Ion drag pumps, Journal of Applied Physics 31 (1) (1960) 136–146.
[9] L. Onsager, Deviations from Ohm's law in weak electrolytes, Journal of Chemical Physics 2 (1934) 539.
[10] J.R. Melcher, Travelling-wave induced electroconvection drag pumps, Physics of Fluids 9 (8) (1966) 1548–1555.
[11] R.V. Raghavan, J. Qin, L.Y. Yeo, J.R. Friend, K. Takemura, S. Yokota, K. Edamura, Electrokinetic actuation of low conductivity dielectric liquids, Sensors & Actuators B 140 (2009) 287–294.
[12] J.R. Melcher, Continuum Electromechanics, MIT Press, Boston, 1981.
[13] D.A. Saville, Electrohydrodynamics: the Taylor-Melcher leaky dielectric model, Annual Review of Fluid Mechanics 29 (1997) 27–64.
[14] L.Y. Yeo, H. Chang, Electrowetting on parallel line electrodes, Physical Review E 73 (2006) 011605.

Biographies

Hideki Yamamoto received his BS degree in mechanical engineering from Keio University, Yokohama, Japan in 2009. He is currently working for his MS degree with the School of Integrated Design Engineering, Keio University.

Kento Mori is an undergraduate student at the Department of Mechanical Engineering, Keio University.

Kenjiro Takemura received his BS degree in mechanical engineering and MS degree in biomedical engineering from Keio University, Yokohama, Japan in 1998 and 2000, respectively. He also received his PhD degree in integrated design engineering from Keio University in 2002. He was with the Department of Mechanical Engineering at Keio University in 2002 as a research associate, and with the Precision and Intelligence Laboratory at Tokyo Institute of Technology as an assistant professor from 2003 to 2008. Since 2008, he has been with the Department of Mechanical Engineering at Keio University where he is currently an assistant professor. He received JSME Young Engineers Award in 2002 for a research on Multi-DOF ultrasonic motor, Best Research Paper Award at the 10th International Conference on Mechatronics Technology in 2006, etc. His research interest is on functional fluids, new actuators/sensors, and mechatronics.

Leslie Yeo is currently an Australian Research Fellow and senior lecturer in the Department of Mechanical & Aerospace Engineering and co-director of the Micro/Nanophysics Research Laboratory at Monash University, Australia. He received his PhD from Imperial College London in 2002, for which he was awarded the Dudley Newitt prize for a computational/theoretical thesis of outstanding merit. Prior to joining Monash University, he was a mathematical modeller at Det Norske Veritas UK and a postdoctoral research associate in the Department of Chemical & Biomolecular Engineering at the University of Notre Dame, USA. Dr. Yeo was the recipient of the 2007 Young Tall Poppy Science Award from the Australian Institute for Policy & Science 'in recognition of the achievements of outstanding young researchers in the sciences including physical, biomedical, applied sciences, engineering and technology, and a finalist in the 2008 Eureka Prize People's Choice Award. Dr. Yeo is the author of over 85 research publications and over 10 patent applications, and is currently the editor of the American Institute of Physics journal Biomicrofluidics.

James Friend received the BS degree in aerospace engineering, and the MS and PhD degrees in mechanical engineering from the University of Missouri-Rolla in 1992, 1994, and 1998, respectively. He received two awards—the AIAA Jefferson Student Goblet and ASME Presentation Award—for his presentation on ultrasonic motor analysis at the AIAA/ASME/AHS/ASC 26th Annual Structural Dynamics Conference in 1996, an award for the encouragement of young scientists at the Symposium for Ultrasonic Electronics and Engineering in 2003 for a presentation on acoustic waveguides, an award in 2004 for a presentation on the Scream actuator at the Spring Meeting of the Acoustical Society of Japan, excellence in teaching and early career researcher awards from the Monash Faculty of Engineering in 2007and 2008, respectively, and a Future Leader award from the Davos Future Summit in Sydney in 2008. James Friend joined Monash University in late 2004, and founded and co-directs the $6.5 million Micro/Nanophysics Research Laboratory with clean room and biolab, a current staff of three academics, three post-doctorates and 13 PhD students. He is an associate professor and deputy head of the Department of Mechanical and Aerospace Engineering at Monash University, with research interests in micro/nanodevices for biomedical applications, with over 100 peer-reviewed publications, with five book chapters, 52 peer-reviewed journal papers, and 13 patents and patent applications.

Shinichi Yokota received his PhD degree in mechanical engineering from Tokyo Institute of Technology in 1982. He was with the Research Laboratory of Precision Machinery and Electronics at Tokyo Institute of Technology as a research associate from 1975 to 1986. Since 1986, he has been with the Precision and Intelligent Laboratory also at Tokyo Institute of Technology, where he is currently a full professor. His research interest is on micro-actuators using functional fluids, micro-machines, and fluid power mechatronics.

Kazuya Edamura received his MS degree in chemical engineering from Tokyo Institute of Technology in 1978. After his career as a chemist in the Research Lab. at Kyowa Hakko Kogyo Co., Ltd. and a Product Manager in Diagnostics Dept., Boehringer Mannheim, Japan, he found the New Technology Management Co., Ltd. His main works are on ECF technology, MRF technology, ERF technology, etc.